Martin Bartsch[a], Zhe-Feng Zhang[b], Christina Scheu[b,c], Manfred Rühle[b], Ulrich Messerschmidt[a]

[a] Max-Planck-Institut für Mikrostrukturphysik, Halle (Saale), Germany
[b] Max-Planck-Institut für Metallforschung, Stuttgart, Germany
[c] Materialprüfungsanstalt, Universität Stuttgart, Stuttgart, Germany

Fracture parameters of chevron-notched Al_2O_3/Nb sandwich specimens

Fracture toughness tests were performed on Al_2O_3/Nb sandwich specimens using chevron-notched bending bars. These tests allow the independent determination of the fracture toughness K_c at a defined crack velocity and the total work of fracture J_c. The J_c values are much greater than the data for the energy release rate G_c following from K_c. The fracture surfaces were studied by optical and scanning electron microscopy. The results are discussed in terms of the fracture toughness of cleavage in the Al_2O_3 and severe plastic deformation in the Nb sheet.

Key words: Metal/ceramic interfaces; Fracture toughness; Plastic deformation; Chevron-notched bending bars

1. Introduction

The experimental work of fracture of metal/ceramic composites along the phase boundary can exceed – by orders of magnitude – the "ideal" fracture energy, i. e. the work of adhesion W_{ad} between the joined materials. This is a consequence of extensive plastic deformation taking place near the crack front. A model system for studying these processes is a composite of single crystals of sapphire and niobium. These materials can be joined by diffusion bonding in ultra-high vacuum to produce crystallographically well-defined and clean interfaces. The relations between the mechanical properties of these interfaces and their atomic and chemical structure are comparably well studied (see, e. g., [1–7]). However, in order to understand the fracture processes in detail, reliable measurements of the fracture parameters are necessary. In comparison to the usually used single-ended notched beam (SENB) bending specimens, bending bars with a chevron notch have a number of advantages:

– A sharp crack grows from the tip of the ligament during loading before the fracture load is determined so that the preparation of specimens with sharp cracks is not necessary.
– The geometry of chevron-notched specimens favours stable crack growth since the line length of the crack increases when the crack proceeds.
– When the fracture load is measured, the crack moves at a well-defined velocity which is related to the loading rate of the testing machine, in contrast to cracks starting to move at SENB tests.
– In addition to the fracture toughness, the total work of fracture can be measured without considering the stored elastic energy since the specimens are fully unloaded at the end of the test.

At present, these advantages are opposed by the shortcoming that the geometry function which is necessary to evaluate the fracture toughness from the maximum load has not yet been calculated for composite samples. Nevertheless, the present study is a first attempt to determine the interface fracture parameters of Al_2O_3/Nb/Al_2O_3 sandwiches from chevron-notched bending specimens. For modelling the fracture behaviour, the flow stress of the soft Nb component and its strain-rate sensitivity are necessary parameters, therefore respective compression tests have also been performed.

2. Experimental

Pure α-Al_2O_3 and Nb single crystals were diffusion bonded in ultra-high vacuum with an apparatus described elsewhere [1, 8]. The bonding was performed at a temperature of 1400 °C and a load of 7 MPa. The bonding time was 3 hours. All specimens of this study were obtained from a single composite block consisting of a 2 mm thick Nb single crystal joined to two 3 mm thick Al_2O_3 single crystal pieces with two different orientation relationships (OR):

A: $(110)_{Nb} \parallel (0001)_{Al2O3}$, $[1\bar{1}0]_{Nb} \parallel [01\bar{1}0]_{Al2O3}$

B: $(110)_{Nb} \parallel (0001)_{Al2O3}$, $[1\bar{1}0]_{Nb} \parallel [2\bar{1}\bar{1}0]_{Al2O3}$

The load direction was always $[1\bar{1}0]_{Nb}$. Two chevron-notched specimens of a length of about 7.7 mm were prepared for each orientation relationship. Preliminary tests were performed on specimens with a polycrystalline Nb foil of 0.3 mm thickness. Figure 1 shows schematically the shape of the specimen cross section in the plane of the chevron notch. The geometrical data of the specimens are listed in Table 1. The notches were cut by a wire saw with a tungsten wire 50 µm in diameter. A special tool was designed to exactly turn the specimens by 36° to produce the cuts on both sides. The cutting wire tended to deviate from the interface plane into the Al_2O_3. This was reduced by guidance bars pushing the wire towards the Nb.

The specimens were loaded in three-point bending in a digitally controlled single-screw testing machine under strain control leading to a high effective stiffness. The load was applied by steel rolls of 1 mm in diameter guided in a cage with $s = 4.2$ mm outer span. The data were recorded

© 2004 Carl Hanser Verlag, Munich, Germany www.hanser.de/mk Not for use in internet or intranet sites. Not for electronic distribution.

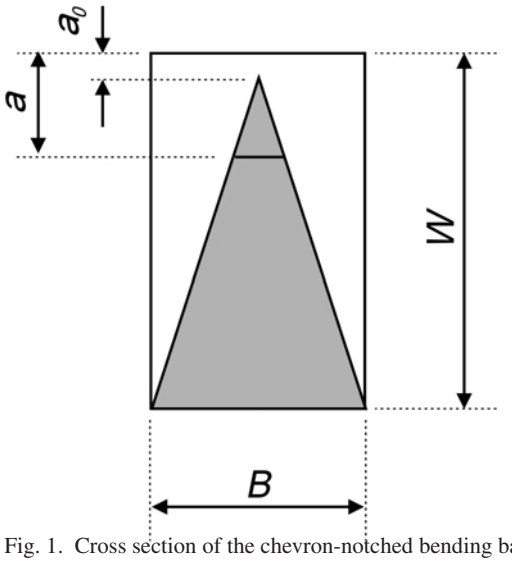

Fig. 1. Cross section of the chevron-notched bending bars.

Table 1. Orientation relationships and geometrical data of chevron-notched bending bars. Exp. Nr.: experiment number; OR: orientation relationship; W: width of specimen; a_0: starting crack length; B: depth of specimen.

Exp. Nr.	OR	W [mm]	a_o [mm]	B [mm]
1	A	2.35	0.66	1.11
3	A	2.09	0.054	1.35
2	B	2.36	0.83	1.00
4	B	2.05	0.027	1.38

in a PC. The fracture surfaces were studied by optical microscopy and scanning electron microscopy (SEM). The SEM measurements were performed with a high-resolution field-emission SEM equipped with an energy-dispersive X-ray spectrometer (EDS).

At the starting material block, the Nb sheet exceeded the outer faces of the sapphire blocks. From this excess Nb material, two compression samples were cut with their loading axes perpendicular to the (110) interfaces, i. e., parallel to the main tensile stress during the fracture tests. These specimens were deformed in compression under constant strain-rate conditions. Strain-rate cycling and stress relaxation tests were carried out to measure the strain-rate sensitivity of the flow stress.

3. Results

3.1. Fracture tests

Figure 2 shows a load-displacement (F vs. d) curve of a preliminary test on a sandwich specimen with a polycrystalline Nb sheet. The specimen was three times partially unloaded and reloaded. It broke in an unstable way. A typical loading curve of a specimen with a Nb single crystal is displayed in Fig. 3. The specimen was unloaded and reloaded at U_1 already during the first stage of increasing load. If the deformation and fracture of the sample were of pure elastic character, the extrapolation of the unloading curve should meet the starting point of the loading curve. The shift of the intercept along the displacement axis indicates irreversible deformation already in this early stage of loading. Afterwards, the curve bends down due to stable crack growth and reaches a maximum with the maximum load F_m which yields the fracture toughness. The respective values are listed in column 3 of Table 2. At the maximum, the specimen was unloaded a second time (U_2). The intercept with the displacement axis has increased resulting from strong plastic deformation during the crack extension. Further unloading-reloading cycles (U_3 and U_4) demonstrate increasing plastic deformation. After reloading from U_2, the fracture load decreases owing to the increasing compliance of the sample. After reloading from U_3, the load remains approximately constant. Apparently, the crack does not proceed during this stage. The stress drop at D corresponds to unstable crack growth.

For chevron-notch fracture tests, the fracture toughness is calculated from the maximum load F_m by

$$K_c = F_m Y^*_{min}/(BW^{1/2}) \quad (1)$$

B is the depth and W the width of the specimens as sketched in Fig. 1. Y^*_{min} is the minimum of the geometry function. Unfortunately, the geometry function is not known for the present sandwich samples. Therefore, the treatment used in [3] is adopted here for the chevron-notched specimens, although a final justification requires calculations by the finite-element method. In [3], it is assumed that the geometry function for a layered composite of the present 1-2-1 form with 1 corresponding to Al_2O_3 and 2 for Nb is a weighted average between that of a bimaterial, Y_{bi}, and that of a layered composite of infinitesimal layer thickness (e. g., [9, 10]). According to the weight function in [3], the geometry function of the present sandwiches with a ratio of the Nb layer thickness to the sample width W of about unity is ap-

Table 2. Fracture data of chevron-notched bending bar fracture tests. Exp. Nr.: experiment number; v: crosshead speed; F_m: maximum load of the load-displacement curve; Y_{min}: minimum of the geometry function of homogeneous chevron-notched bending bars; K_c: critical stress intensity factor from F_m by Eqs. (1) to (5); G_c: critical energy release rate from K_c by Eqs. (6) and (7); J_c: J integral from total area under the load-displacement curve; da/dt: crack velocity.

1	2	3	4	5	6	7	8
Exp. Nr.	v [μm s^{-1}]	F_m [N]	Y_{min}	K_c [MPam$^{1/2}$]	G_c [J m^{-2}]	J_c [J m^{-2}]	da/dt [μm s^{-1}]
1	0.2/1/2	42.6	9.17	7.04	304	2603	55
3	1	71.4	6.46	7.25	322	764	391
2	0.2/2	31.9	10.4	6.62	269	809	56
4	1	97.4	6.45	9.75	583	1551	288

© 2004 Carl Hanser Verlag, Munich, Germany www.hanser.de/mk Not for use in internet or intranet sites. Not for electronic distribution.

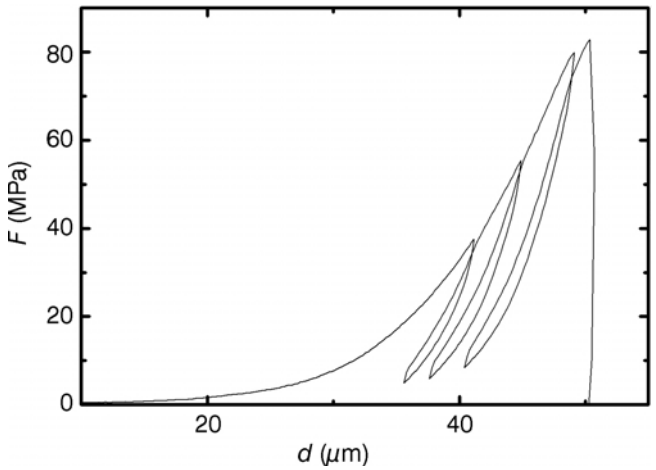

Fig. 2. Load-displacement curve of a fracture test performed on a sandwich sample with a polycrystalline Nb sheet.

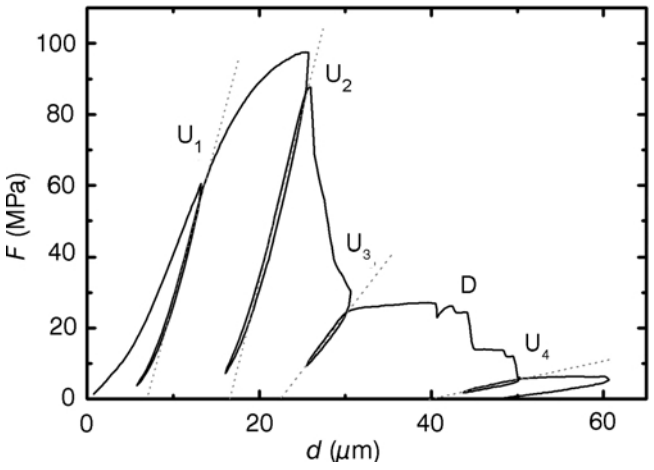

Fig. 3. Load-displacement curve of a specimen with OR B.

proximately equal to that of the bimaterial, i. e.,

$$Y^*_{\min} \cong Y_{\mathrm{bi}} = (1-\beta^2)\,(1+4\varepsilon^2)\,Y_{\min} \tag{2}$$

where

$$\beta = \frac{\mu_1[1-2\nu_1] - \mu_2[1-2\nu_2]}{\mu_1[1-\nu_1] + \mu_2[1-\nu_2]} \tag{3}$$

is the second of the so-called Dundurs' parameters [9, 11] and ε the oscillation index

$$\varepsilon = (1/2\pi)\ln[(1-\beta)/(1+\beta)] \tag{4}$$

μ_i and ν_i are the shear moduli and Poisson's ratios of the constituents of the specimens, and

$$Y_{\min} = [3.08 + 5(a_o/W) + 8.33(a_o/W)^2]\,(s/W) \tag{5}$$

is the minimum of the geometry function for homogeneous chevron-notched specimens under three-point bending [12]. According to Table A1 in [3], $\beta = 0.214$ (note the different signs in Eq. (3) and in [3]) and $\varepsilon = -0.069$ for the present materials and orientation relation B. Thus, $Y^*_{\min} = 0.97\,Y_{\min}$, i. e., the geometry function of the composite specimens does not differ much from that of the usual homogeneous specimens. The values of $Y_{\min}$ and the resulting values of K_c are listed in columns 4 and 5 of Table 2. The displacement rates $v = \mathrm{d}d/\mathrm{d}t$ are displayed in column 2. In the experiments starting with the small displacement rate of 0.2 μm s^{-1}, the rate was increased by factors of 5 or 10 near the end of the experiments. Although the K_c values scatter, a distinct difference between the orientation relationships A and B or the different displacement rates was not observed.

Using linear elastic fracture mechanics, the K_c values can be converted into energy-release rates by

$$G_c = K_c^2/E^* \tag{6}$$

where

$$E^* = \frac{2E_1E_2}{E_2(1-\nu_1^2) + E_1(1-\nu_2^2)} \tag{7}$$

is the effective elastic modulus of the bicrystal and E_i are the moduli of the constituents. According to Table A1 in [3], $E^* = 163$ GPa for the present materials and orientation relationship B. The values of G_c are shown in column 6 of Table 2.

By means of chevron-notch fracture tests, the total fracture energy J_c can easily be determined from the integral over the loading curve as in Fig. 3 divided by the fracture area taken from optical micrographs. The data obtained are listed in column 7 of Table 2. If the specimens are deformed until total fracture, the elastic energy stored during loading is completely released and need not be considered. In the present study, some specimens like that in Fig. 3 were unloaded before total fracture occurred. In these cases, the J_c values of Table 2 underestimate the true values by a few per cent. The total fracture energies J_c are greater than the G_c values calculated from the fracture toughness K_c by factors of about 2 to 7 and they scatter much more than the K_c values.

In chevron-notch fracture tests with a linear elastic fracture behaviour, a clear relation between the stable crack growth rate $\mathrm{d}a/\mathrm{d}t$ and the drive rate of the testing machine $v = \mathrm{d}d/\mathrm{d}t$ (e. g., [13]) exists at the maximum of the loading curve

$$\frac{\mathrm{d}a}{\mathrm{d}t} = \frac{F_m}{2G_c b}\frac{\mathrm{d}d}{\mathrm{d}t} \tag{8}$$

b is the line length of the crack at the load maximum. For $a_o = 0.2W$, which is only roughly fulfilled at the present specimens, $Y_{\min}$ is reached at $a = 0.37W$ so that $b = 0.21B$. Using this result and the G_c data of column 6 of Table 2 yields the crack growth rates $\mathrm{d}a/\mathrm{d}t$ at the load maximum listed in column 8.

The fracture surfaces were studied by optical and scanning electron microscopy. Preliminary tests on specimens with a polycrystalline Nb layer revealed fracture surfaces which are smooth and run along the interface. In contrast, for the single-crystalline specimens rough fracture surfaces were found. Figure 4 presents an optical micrograph of the Al_2O_3 side of a specimen of orientation relationship A. This fracture surface was further investigated in the SEM (Fig. 5) where the chemical composition of the different areas was analysed by EDS. The fracture occurred mainly inside the Al_2O_3, except within the small bright areas in Fig. 4 or the smooth ones in Fig. 5 labelled by arrows. These were identified as Nb regions indicating that in these areas the crack is running at the interface or in the Nb close to it.

© 2004 Carl Hanser Verlag, Munich, Germany www.hanser.de/mk Not for use in internet or intranet sites. Not for electronic distribution.

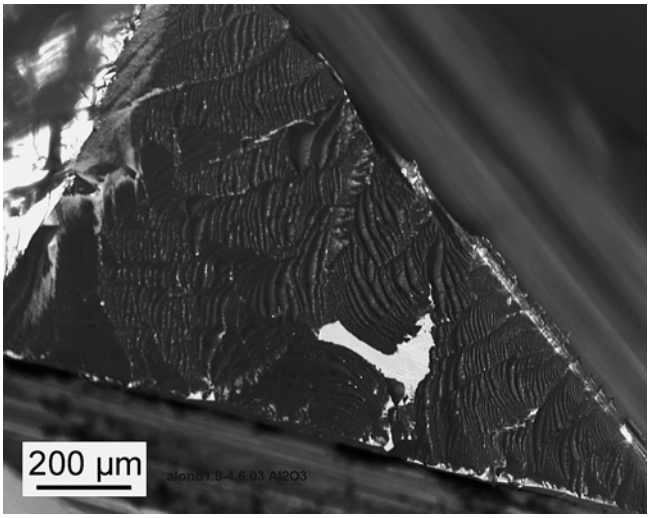

Fig. 4. Optical micrograph of the Al_2O_3 side of a specimen with OR A.

In all other investigated single-crystalline specimens, the crack moved only inside the Al_2O_3. Figure 6 displays SEM micrographs of the Nb side of a specimen with orientation relationship B taken at different magnifications. The fracture surfaces are very rough and consist of cleavage faces different from the $(0001)_{Al2O3}$ interface planes. As shown in Fig. 6a, the cleavage faces intersect on lines appearing along the three $\langle 1\bar{1}00\rangle$ directions in the projection onto the $(0001)_{Al2O3}$ image face. This is consistent with $\{1\bar{1}0n\}$ cleavage faces, probably the $\{1\bar{1}02\}$ faces indicated in Fig. 6a and listed in [6], based on data from [14]. Figure 6b shows an area from the left side of Fig. 6a in high magnification indicating that the cleavage steps are frequently very fine.

3.2. Plastic deformation tests

As described in Section 2, for uniaxial compression tests two specimens were prepared from the starting sandwich material block with a $\langle 110\rangle$ loading axis perpendicular to the interface in the fracture specimens. A typical stress–strain curve is displayed in Fig. 7. σ and ε are the technical flow stresses and strains, respectively. The average yield stress is $\sigma_y = 84$ MPa. The work-hardening coefficient is $\Theta \cong 1$ GPa. The strain rate sensitivity r of the flow stress was measured by strain-rate cycling experiments according to

$$r = \Delta\sigma/\Delta \ln \dot{\varepsilon} \quad (9)$$

In addition, a few stress relaxation experiments were performed. The logarithm of the relaxation rate $-\dot{\sigma}$ was plotted versus the stress σ. The reciprocal slope of these plots is the strain rate sensitivity

$$r = \Delta\sigma/\Delta \ln (-\dot{\sigma}) \quad (10)$$

The relaxation curves are almost straight over more than two orders of magnitude of the strain rate, indicating only a weak dependence of r on $\dot{\varepsilon}$. As shown in Fig. 8, r decreases weakly with increasing plastic strain. The strain rate sensitivity can also be expressed by the so-called stress exponent

$$m^* = \mathrm{d} \ln \dot{\varepsilon}/\mathrm{d} \ln \sigma = \sigma/r \quad (11)$$

The stress exponents increase from about 17 at low strains to 27 at. 2 %.

4. Discussion

At first, the fracture mode is discussed. Specimens with the orientation relationships A and B exhibit the strongest interfaces of those samples studied in [3–7]. According to this literature, they have a similar fracture energy of about 1900 J/m^2, which is much higher than the fracture

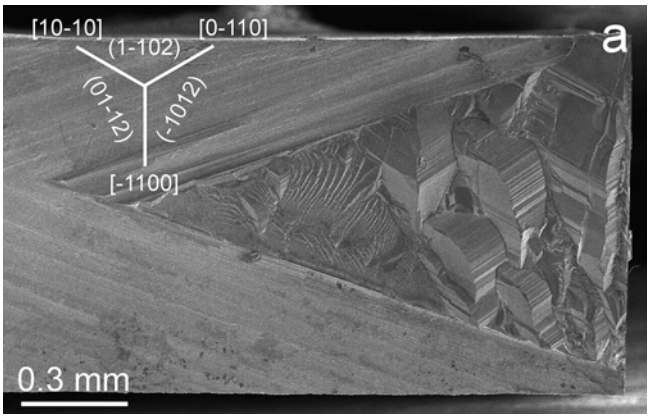

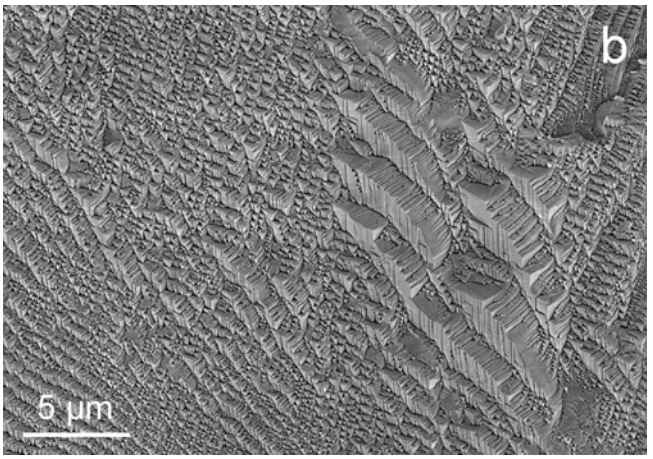

Fig. 6. SEM micrographs of the Nb side of a sample with OR B after the chevron test. (a) Overview and (b) section with fine cleavage steps in high magnification.

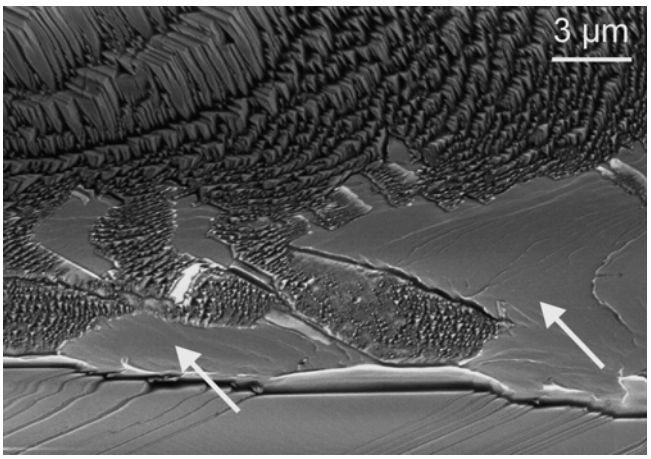

Fig. 5. High magnification SEM image of the Nb side a sample with OR A after the chevron test.

© 2004 Carl Hanser Verlag, Munich, Germany www.hanser.de/mk Not for use in internet or intranet sites. Not for electronic distribution.

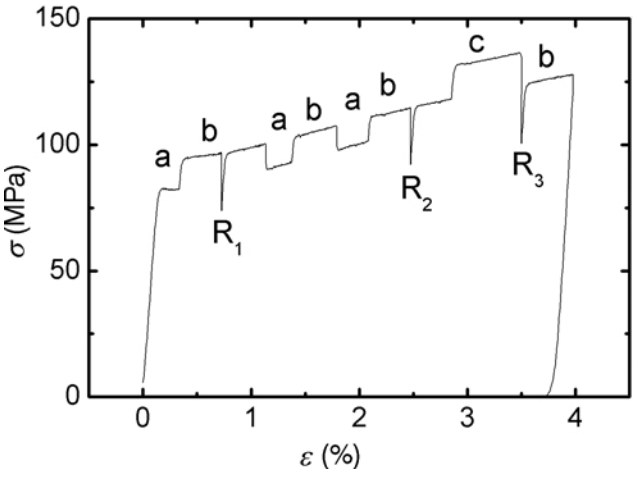

Fig. 7. Stress–strain curve of an Nb specimen along a ⟨110⟩ compression axis at room temperature. Strain-rate cycling experiments were performed between the strain rates $\dot{\varepsilon} = 10^{-5}\ s^{-1}$ (a), $10^{-4}\ s^{-1}$ (b), and $10^{-3}\ s^{-1}$ (c). Stress relaxation tests at R_1 to R_3.

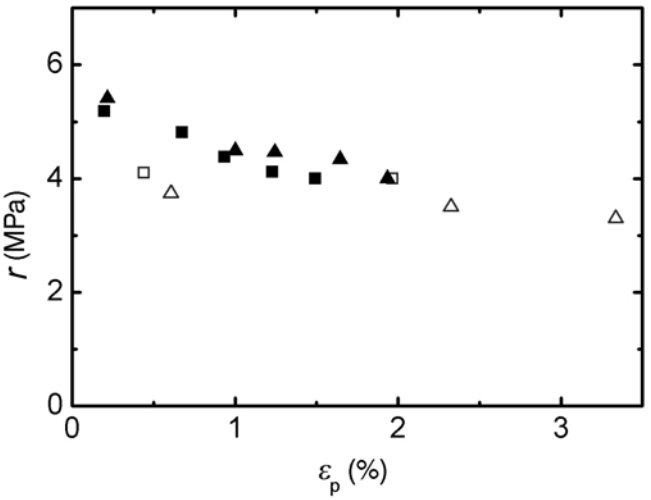

Fig. 8. Strain-rate sensitivity versus plastic strain. Squares and triangles correspond to different specimens, full symbols to strain-rate cycling tests between 10^{-5} and $10^{-4}\ s^{-1}$ and open symbols to stress relaxation tests.

energies of specimens with different crystallographic orientation relationships, e. g. $(111)_{Nb} \parallel (0001)_{Al2O3}$, $[\bar{1}\bar{1}2]_{Nb} \parallel [01\bar{1}0]_{Al2O3}$, where values of around 100 J/m^2 were found [5–7]. Because of the high interface strength, the present specimens broke within the Al_2O_3, which was originally not intended. However, specimens with the respective orientation relationship in [3] failed along the interface only if the interface strength was reduced by doping with Ag. Since the fracture occurred within the Al_2O_3, the fracture data of the composite specimens should be compared with those of α-Al_2O_3 single crystals. Literature data of the fracture toughness K_{Ic} are 5.62 MPa m$^{1/2}$ [13] or >40 MPa m$^{1/2}$ [14] for the (0001) fracture plane and <3 MPa m$^{1/2}$ [13] or about 7 MPa m$^{1/2}$ [14] for prism and pyramidal planes. Thus, the present (0001) interface plane has the highest fracture resistance in Al_2O_3 so that the crack deviates onto other fracture planes of lower fracture resistance resulting in the observed rough fracture surfaces (Figs. 4–6). The fracture toughness data of the present study, column 5 of Table 2, are of the order of the 7 MPa m$^{1/2}$ [14] for the pyramidal cleavage faces observed experimentally. Nevertheless, there occurs already irreversible deformation as indicated by the shift of the intercept of the unloading curves with the displacement axis away from the origin, even in the early stages of the fracture tests.

Following the treatment in [3], the K_c values were converted into energy release rates G_c using Eqs. (6) and (7) on the assumption that the formulae from linear elastic fracture mechanics can be applied. The present values of column 6 of Table 2 are considerably higher than the respective value of about 100 J m^{-2} from [3] (Fig. 6d therein) for the undoped interface with orientation relationship B. One reason may be the different crack-growth rates. In the present study, near the load maximum, the cracks moved in a stable way at well defined velocities of about 55 and 340 μm s^{-1} (column 8 in Table 2). This is by a factor of more than 100 smaller compared to the maximum crack velocity estimated in [3]. The fracture process in the Al_2O_3 should not be very rate dependent. Even if there are plastic processes in the Nb involved at the load maximum, the strain rate sensitivity of the flow stress of Nb – expressed by the stress exponents m^* around 22 – indicates only a moderate strain-rate sensitivity of the plastic deformation, which should not result in an increase of G_c by factors of 2.7 to 5.8 owing to a reduction of the crack-growth rate by a factor of 100.

The K_c or G_c values describe the force necessary to extend the crack. In contrast to this, J_c measures the total energy necessary to form the crack which includes also the energy spent for plastic deformation far away from the crack. Accordingly, the J_c values of column 7 of Table 2 are much greater than the respective G_c values indicating excessive plastic deformation. This conclusion can be supported by an estimation of the size of the plastic zone of the crack. Using a relation for homogeneous materials [15], which is approximately valid also for the present bicrystal geometry [16, 17], the radius of the plastic zone is

$$r_y = \frac{GE^*}{2\pi\sigma_y^2} = \frac{1}{2\pi}\left(\frac{K_c}{\sigma_y}\right)^2 \qquad (12)$$

With the K_c values from column 5 of Table 3 and the flow stress σ_y = 84 MPa, the radius of the plastic zone is between about 1 and 2.1 mm. Thus, plastic deformation may occur in the whole Nb sheet.

5. Conclusions

- For the first time, fracture tests using chevron-notched bending bars were performed on specimens with metal/ceramic interfaces. These tests are well suited to measure the fracture toughness at defined crack velocities.
- Al_2O_3/Nb interfaces with $(110)_{Nb} \parallel (0001)_{Al2O3}$ are very strong so that the specimens mostly break inside the Al_2O_3. The measured fracture toughness K_c is approximately equal to literature data for cleavage along the pyramidal faces observed by scanning electron microscopy.
- The total work of fracture J_c is much greater than the G_c value following from K_c, suggesting that plastic deformation occurs in the whole Nb sheet also far from the crack tip.

© 2004 Carl Hanser Verlag, Munich, Germany www.hanser.de/mk Not for use in internet or intranet sites. Not for electronic distribution.

The authors thank Prof. Frank Ernst for his contribution to the project application. Financial support by the Deutsche Forschungsgemeinschaft (DFG) is gratefully acknowledged.

References

[1] D. Korn, G. Elssner, H.F. Fischmeister, M. Rühle: Acta Metall. Mater. 40 (1992) S355.
[2] G. Elssner, D. Korn, M. Rühle: Scripta Metall. Mater. 31 (1994) 1037.
[3] D. Korn, G. Elssner, R.M. Cannon, M. Rühle: Acta Mater. 50 (2002) 3881.
[4] R.M. Cannon, D. Korn, G. Elssner, M. Rühle: Acta Mater. 50 (2002) 3903.
[5] G. Soyez, G. Elssner, M. Rühle, R. Raj: Acta Mater. 46 (1998) 3571.
[6] G. Soyez, G. Elssner, M. Rühle, R. Raj: J. Mater. Sci. 35 (2000) 1087.
[7] G. Soyez: PhD Thesis, University of Stuttgart, 1996.
[8] W. Kurtz: Z. Metallkd. 93 (2002) 432.
[9] T. Suga, G. Elssner, S. Schmauder: J. Comp. Mater. 22 (1988) 917.
[10] J.W. Hutchinson, Z. Suo: Adv. Appl. Mech. 29 (1992) 63.
[11] J. Dundurs: J. Appl. Mech. 36 (1969) 650.
[12] D. Munz, R.T. Bubsey, J.L. Shannon, Jr.: J. Am. Ceram. Soc. 63 (1980) 300.
[13] J. Tatami, K. Yasuda, Y. Matuso, S. Kimura: Proc. Ceram. Soc. Japan, Annual Meeting 2B (1996) 23, quoted in: W. Wunderlich, H. Awaji, Mater. Design 22 (2001) 53.
[14] S.M. Wiederhorn: J. Am. Ceram. Soc. 52 (1969) 485.
[15] C.F. Shih: J. Mech. Phys. Solids 29 (1981) 305.
[16] C.F. Shih: S. Suresh, Scripta Metall. Mater. 25 (1991) 1017.
[17] C.F. Shih: Mater. Sci. Eng. A143 (1991) 77.

(Received June 1, 2004; accepted July 5, 2004)

Correspondence address

Prof. U. Messerschmidt
MPI für Mikrostrukturphysik
Weinberg 2, D-06120 Halle (Saale), Germany
Tel.: +49 345 5582 927
Fax: +49 345 5511 223
E-mail: um@mpi-halle.de

© 2004 Carl Hanser Verlag, Munich, Germany www.hanser.de/mk Not for use in internet or intranet sites. Not for electronic distribution.